Optimization Framework for Low-Thrust Active Debris Removal Missions with Multiple Selected Targets

Joanna Hon
Turion Space Corporation
M. Reza Emami
University of Toronto Institute for Aerospace Studies

ABSTRACT

Optimal planning for multi-target rendezvous missions consists of a combinatorial optimization problem for debris target sequencing, coupled with a continuous, nonlinear optimization problem for trajectory planning. The problem is formulated as a variant of the time-dependent travelling salesman problem, whereby the objective function to minimize is the total mission ΔV provided a set of mission constraints. A three-stage framework is developed to perform this optimization for low-thrust active debris removal missions targeting debris objects in both circular and elliptical orbits. The first stage generates a two-dimensional approximation of the time-dependent search space for each departure-arrival debris pair using a combination of analytical estimation methods and a Q-law inspired guidance scheme. The second stage employs a genetic algorithm to search the discretized problem space and optimally sequence the debris object list. Finally, the last stage implements a gradient-based time-varying controller to tune the gains in the Lyapunov candidate function to refine the trajectory optimization, provided the converged debris object sequence. The debris sequence, maneuver epoch, thrust vector time history, and total ΔV cost to remove select debris objects considering the J_2 perturbation are outputs of this optimization framework. The validity of the proposed framework is demonstrated through three ADR case studies. The outcome of this research is a flexible tool for the optimal planning of low-thrust active debris removal missions.

1. INTRODUCTION

Numerical studies on the evolution of space debris population in low-Earth orbit (LEO) have indicated that even in the absence of future launch activities, the population is unstable, making its growth inevitable [1]. As the rate of naturally decaying debris objects is slower than the stabilizing 5-10 debris removal rate [2], active debris removal (ADR) missions will perform a vital function in sustaining the space environment for ongoing and future operations. Spacecraft-based debris remediation strategies that remove multiple objects with a single mission are of considerable interest due to their high utility and economic feasibility. Further reduction in mission costs can be achieved by optimizing the debris sequencing and rendezvous trajectories to minimize propellant consumption. This problem, coined the multi-target rendezvous problem (MTRV), thus consists of 1) a combinatorial optimization for debris target sequencing, and 2) a continuous, nonlinear optimization for trajectory planning [3].

The duality of the MTRV problem is made complex by the presence of J_2. The Earth's oblateness perturbation changes the orientation of an orbit over time, doing so at a rate that depends on the semimajor axis, eccentricity, and inclination of the orbit. As a result, the maneuver cost for the chaser spacecraft to transfer from one target to another largely depends on the departure and arrival epoch. In efforts to simplify the problem and render it more computationally tractable, some researchers have optimized ADR sequences using the assumption of static transfer costs. This assumption is valid if the debris targets of interest reside in very similar orbit planes [4], or if the transfer maneuvers are executed after the chaser spacecraft drifts to an orbit that satisfies a predefined criteria bounding the ΔV required [5, 6, 7]. This simplification is appropriate for ADR missions designed to remove the maximum number of objects from a large catalog of debris options, as would exist in debris clouds. However, one may be interested in designing an ADR mission to maximize the stabilizing impact on the LEO population by removing specific, high-priority debris targets. Optimal planning for these missions would require a different transfer strategy whose maneuver costs evolve with time, as close alignment of orbits may only occur between some debris objects with variable frequency within

the mission window. As a result, the MTRV problem for these ADR missions is necessarily formulated as a variant of the time-dependent travelling salesman problem (TD-TSP) [8].

Due to their superior I_{sp}, a measure of propellant efficiency, using low-thrust propulsion for ADR missions can enable the removal of a broader range and larger volume of debris objects. Despite this performance advantage, only a handful of studies have considered optimizing the MTRV problem with low-thrust maneuvers. This is because low thrust orbital maneuvers in LEO require many-revolution transfers, which alone, present a challenging optimal control problem for trajectory optimization. Zuiani and Vasile approached the MTRV optimization problem for ADR missions that use low thrust propulsion with a simplified many-revolution transfer model [9]. This model is based on the 1st order solution of perturbed Keplerian motion, in which spacecraft thrust was the only perturbation assumed and the effect of J_2 was neglected. The study conducted by Di Carlo et al. accounted for the contribution of the J_2 zonal harmonic in their low-thrust transfer model but assumed transfer time independence [4]. Li et al. [10] re-derived Edelbaum's analytical ΔV estimation for low-thrust maneuvers to include the J_2 perturbation and RAAN changes. Cerf also used this analytical formulation for their low-thrust propulsion ADR case study [11]. However, Edelbaum's work assumes continuous thrusting, which corresponds to minimizing transfer time rather than ΔV [12]. To the author's knowledge, no studies have proposed to optimize the MTRV problem with low-thrust propulsion with a J_2-perturbed dynamic model under a framework that accounts for the time-dependent nature of trajectory optimization and applies a transfer strategy that minimizes ΔV instead of transfer time. Furthermore, the debris orbits in previously conducted MTRV studies have largely been circular.

Both deterministic and stochastic algorithms have been used to optimize the debris sequencing aspect of the MTRV problem. Of the deterministic approaches, Braun et al. explored fixed-length rendezvous sequences using a brute-force approach [13] and Yu et al. pursued a hybrid optimal control framework, in which the sequence optimization was performed using an exhaustive search [14]. These methods can work reasonably well to optimally sequence the 4-5 objects that were considered in the studies, but quickly become computational impractical at solving large-scale cases. Tree search algorithms such as the brand-and-bound method used by Berend et al. [5] and Yang et al. [15] can reduce the computational load required by pruning nodes at each level of the search process, retaining only those that look promising. However, it is possible to prematurely prune excellent solutions during the search process. Relaxation of the pruning condition can be used to decrease this risk, but the computational load increases accordingly. To contrast deterministic approaches, stochastic metaheuristics are more efficient at finding near-optimal solutions for large-scale optimization problems. These methods avoid enumerating through all feasible combinations, and instead search the solution space using random variables and probability functions guided by a higher-level convergence procedure. This allows stochastic metaheuristics to explore the solution space efficiently and approximate the global optimum with high probability. It is possible to hybridize a metaheuristic with deterministic algorithms to improve local search procedures. Hybridization of the two broad optimization techniques have been used by Zuiana et al. [9] and Chen et al. [7] in their optimal mission planning studies. Other optimization algorithms used include Simulated Annealing (SA) [11], Genetic Algorithm (GA) [16], Ant Colony Optimization (ACO) [17, 7, 3], and Particle Swarm Optimization (PSO) [18]. SA is a single-solution metaheuristic approach that focuses on modifying and improving a single candidate solution. This is in contrast with the latter three listed methods (GA, ACO, PSO), which maintain and improve multiple candidate solutions, using either collective behavior or population characteristics to guide the search. As the solution space grows factorially with the number of debris objects to sequence, a population-based metaheuristic is employed in this research to globally optimize the MTRV problem.

In the present paper, a modular framework is presented to optimize the MTRV problem for ADR missions targeting debris in both circular and elliptical orbits using low-thrust chaser spacecraft. The methodology consists of three stages. The first stage generates a two-dimensional approximation of the time-dependent search space for each departure-arrival debris pair using a combination of analytical estimation methods and a Q-law inspired guidance scheme. The second stage employs a genetic algorithm to search the discretized solution space and optimally sequence the debris object list. Finally, the last stage implements a gradient-based time-varying controller to tune the gains in the Lyapunov candidate function to refine the trajectory optimization, provided the converged debris object sequence. Mission window constraints, transfer strategy, and an upper bound on object-to-object transfer times are identified to bound the optimization problem. The trajectory optimization will be conducted for long-range rendezvous maneuvers, while the time required for proximity operations are accounted for. The effects due to J_2 perturbation are included in the dynamic description of the problem. The debris sequence, maneuver epoch, and thrust vector are established as problem variables, while the total maneuver cost (ΔV and transfer time) is the design objective to minimize. The convergence performance, robustness, and validity of the framework is demonstrated with 3 distinct ADR case studies. The results

demonstrate that the proposed transfer strategy and the use of low-thrust propulsion systems can enable the removal of a broader range of debris objects, at a lower $ cost per kg. The final product is an optimal mission planning tool for ADR missions targeting debris in low-Earth orbit.

The organization of this paper is as follows. A description of the global optimization problem is presented in Section 2. The methods used to estimate the ΔV of a variety of low-thrust transfer strategies are outlined with the dynamic model in Section 3. The optimization approach and algorithms will then be explained in Section 4. Finally, the results of three ADR case studies is provided in Section 5 to demonstrate the effectiveness of the developed framework.

2. GLOBAL OPTIMIZATION PROBLEM DEFINITION

Optimization of this problem is defined as minimizing the total ΔV required to completely remove a defined set of debris objects in LEO within the allocated mission window. For the purposes of designing this framework, the debris set shall be considered as an arbitrary collection of debris objects, as the debris target selection is outside the scope of this study. The ADR mission concept is modelled after the overall concept for the Deorbiter CubeSat mission [19]. This ADR mission uses a mothership chaser spacecraft to carry and deploy several debris-removal nanosatellites, called Deorbiter CubeSats. The mothership spacecraft is responsible for transporting the Deorbiter CubeSats near the vicinity of predetermined debris objects and for characterizing the dynamical state of these target debris prior to Deorbiter deployment. This is achieved via two sets of maneuvers: a long-range maneuver and formation flying. As the ΔV required to perform formation flying is largely independent of the debris sequence, only its duration and the ΔV required by the long-range maneuver is accounted for in this framework.

There are a variety of low-thrust transfer strategies available, and their comparative optimality depend on the shape and relative orientation of the initial and target orbits [12] [10] [20] [21] [22]. To avoid reducing the solution space prematurely and lose potential optimums, let Φ denote the family of functions $\{\phi_1, \phi_2, ...\phi_k\}$ corresponding to k viable low-thrust transfer strategies considered in this study. The given MTRV problem can thus be represented by the directed graph $\mathbf{G} = (\mathbf{V},\ \mathbf{A})$ where $\mathbf{V} = \{1, 2, 3... \ n\}$ is the set of nodes corresponding to n debris targets and $\mathbf{A}$ is the set of arcs defined by Eq. 1, representing all the possible transfer maneuvers between each ordered debris pair.

$$\mathbf{A} \coloneqq \{a_{ijk} = \phi_k(ij) \mid ij \in \mathbf{V} \times \mathbf{V},\ i \neq j\} \qquad \forall\ \phi_k \in \Phi \tag{1}$$

As a result, there exist four sets of decision variables for this problem. There is the binary variable $x_{ij} \in \mathbf{x}$ that takes the value of 1 when the chaser transfers from debris i to debris j and 0 otherwise; there is the discrete variable $k \leq |\Phi|$, $k \in \mathbb{N}^*$ that selects the transfer strategy $\phi_k \in \Phi$ to rendezvous with debris j from debris i; and there are the variables $t_{a,i} \in \tau_a$ and $t_{d,i} \in \tau_d$ denoting the arrival and departure epochs to and from target i, respectively. The variable representing the transfer costs, $c_{ijk}(t_{d,i},\ t_{a,j},\ \phi_k)$, is thus a function of the transfer strategy, the departure and arrival epochs from and to targets i and j, summarizing the dynamic nature of this TSP variant.

The specifics regarding mission window, maneuver duration, and spacecraft specifications shall be made adjustable to accommodate different mission scenarios. Let the start of the mission correspond with the time when the mothership arrives in near the vicinity of the first debris in the sequence. Then, the constraints bounding this problem are:

1. All debris targets $\in \mathbf{V}$ shall be removed by a Deorbiter CubeSat deployed by the mothership
2. They should all be removed within the specified the mission window $\left[T_0,\ T_f\right]$.
3. The flight time for each long-range rendezvous transfer leg shall not exceed ToF_{max}.
4. The duration between contiguous transfer maneuvers shall be at least the time required for formation flying, Δt_{serv}, an interval defined by that required to achieve sufficient dynamical characterization of the target debris.
5. There is an upper limited on the total achievable ΔV_{max} for each mission, as determined by a maximum mass ratio $\frac{m_0}{m_{f_{min}}}$ for the chaser spacecraft.

As the group of permutations of $\mathbf{V}$, $\mathbf{S}(\mathbf{V})$, represents the set of solution candidates of the MTRV problem, the optimal

solution of the MTRV problem is thus defined as the rendezvous sequence S^* with transfer trajectories that achieves:

$$\min_{x,\tau_a,\tau_d,\Phi} C = \sum_{i\in V}\sum_{j\in V} c_{ijk}(t_{d,i},\ t_{a,j},\ \phi_k)\ x_{ij} \tag{2}$$

subject to

$$\sum_{i\in V} x_{ij} = 1, \qquad \forall\ j \in \mathbf{V} \tag{3}$$

$$\sum_{j\in V} x_{ij} = 1, \qquad \forall\ i \in \mathbf{V} \tag{4}$$

$$x_{ij} \in \{0,\ 1\} \qquad \forall\ ij \in \mathbf{V}\times\mathbf{V},\ i \neq j \tag{5}$$

$$t_{a,i} + \Delta t_{serv} \leq t_{d,i} \qquad \forall\ i \in \mathbf{V} \tag{6}$$

$$t_{a,j} - t_{d,i} \leq ToF_{max} \qquad \forall\ ij \in \mathbf{V}\times\mathbf{V},\ i \neq j \tag{7}$$

$$m(t_{a,i}) - m(t_{a,i} + \Delta t_{serv}) = m_{deorbiter} \qquad \forall\ i \in \mathbf{V} \tag{8}$$

$$t_{a,1} = T_0 \tag{9}$$

$$m(T_0) = m_0 \tag{10}$$

$$t_{a,n} + \Delta t_{serv} = t_f \leq T_f \qquad n = |\mathbf{V}| \tag{11}$$

$$m(t_f) \geq m_{f_{min}} \tag{12}$$

3. SYSTEM DYNAMIC MODEL

To remain flexible to the volume and type of debris this framework can optimize, the methods used to describe the dynamics shall be general, yet computationally efficient. As a result, it is desirable to use an analytical model to approximate the minimum ΔV required, wherever possible, and to use an efficient guidance algorithm where it is not. In this study, four transfer strategies are implemented in the optimization framework, corresponding to $|\Phi| = 4$ for the global optimization problem.

3.1 Analytical Methods for Circular Orbits

Most analytical models for low-thrust transfers build off Edelbaum's work [10], which ultimately provide a minimum time solution rather than minimum ΔV due to the necessary assumption of constant thrust. As the objective of the trajectory optimization scheme is to approximate a minimum ΔV solution, the transfer strategy for this framework should be based off an analytical model that does not require constant thrust to estimate the transfer cost. Luckily, Di Carlo and Vasile have proposed such a model in their 2021 study [20]. In this paper, the researchers derived analytical solutions for the two-point boundary value problem (TPBVP) of a low-thrust transfer between two circular Earth-centered orbits under the effect of J_2. In this derivation, it is assumed that the perturbing force provided by the propulsion system is sufficiently low "*to produce negligible variations in the orbital elements over one orbital period*". This enables the use of constant orbit averaged values in their formulations. The result of this referenced work are analytical formulations that, when initialized as a feasible TPBVP, accurately estimate the ΔV required by three different low-thrust long-range transfer strategies. Each of the transfer strategies are split into 2 phases, in which different sets of orbital elements are modified. Adopting the notation in [20], these strategies are summarized below.

Strategy 1, ϕ_1: $[\Delta\Omega_{J_2}, (\Delta\bar{a}, \Delta\bar{i})]$. First, exploit the effects of J_2 on the evolution of the orbital plane and drift to a RAAN that is closer to the target debris orbit. Then, low-thrust is applied along two thrust arcs that span an angle of $2\bar{\psi}$ with a constant elevation angle $\bar{\beta}$. These thrust arcs are centered at the nodal points of the orbit. The change in Ω in the first phase is tuned such that additional Ω variation as a result of the second phase achieves the target $\bar{\Omega}_f$. It was observed that for a given time of flight, the TPBVP is a nonlinear function of $\bar{\psi}$ alone. A nonlinear solver was used to calculate this parameter and the solution is fed into Equation 13 to find the ΔV of the transfer.

$$\Delta V_{\phi_1} = \left(\sqrt{\frac{\mu}{\bar{a}_0}} - \sqrt{\frac{\mu}{\bar{a}_f}}\right)\sqrt{1 + \frac{4\bar{\psi}^2(\bar{i}_f - \bar{i}_0)^2}{\sin^2\bar{\psi}\log^2(\bar{a}_f/\bar{a}_0)}} \tag{13}$$

Strategy 2, ϕ_2: $[(\Delta\bar{a}, \Delta\bar{i}), \Delta\Omega_\beta]$. The second strategy reverses the order of which the sets of orbital elements are varied. Additionally, rather than using a drift orbit to achieve the desired $\Delta\bar{\Omega}$, the RAAN is adjusted with a low-thrust maneuver in the second phase as well. The first phase of this transfer strategy is identical to the second phase of

ϕ_1. This maneuver proceeds for a duration of ToF_1. In the second phase, thrust is applied entirely out-of-plane over another two constant $2\bar{\psi}_2$ arcs for ToF_2 to arrive to the destination $\bar{\Omega}_f$. Unlike the first transfer strategy, this transfer strategy possesses two independent control variables to solve for, requiring two inputs to bound the nonlinear problem. Thus, the control parameters of this strategy, $\{\bar{\psi}_1,\ \bar{\psi}_2\}$ are solved numerically via time-discretization. The ΔV of this transfer is highlighted in Eq. 14, where ε refers to the spacecraft acceleration due to thrust.

$$\Delta V_{\phi_2} = \left(\sqrt{\frac{\mu}{\bar{a}_0}} - \sqrt{\frac{\mu}{\bar{a}_f}}\right)\sqrt{1 + \frac{4\bar{\psi}_2{}^2(\bar{i}_f - \bar{i}_0)^2}{\sin^2\bar{\psi}_2 \log^2(\bar{a}_f/\bar{a}_0)}} + \frac{2\varepsilon\bar{\psi}_2}{\pi} ToF_2 \tag{14}$$

Strategy 3, ϕ_3: $[(\Delta\bar{a}, \Delta\Omega_{J_2}), \Delta\bar{i}]$. In this transfer strategy, tangential thrust ($\bar{\beta} = 0$) is applied over two constant arcs of $2\bar{\psi}_1$ centered at the nodes to achieve the desired $\Delta\bar{a}$. In the second phase, thrust is applied entirely out-of-plane to arrive at $\bar{i}_f$. The variation in $\bar{\Omega}$ is entirely due to the J_2 effect, so the $\Delta\bar{\Omega}_1$ realized in the first phase must be compatible with the $\Delta\bar{\Omega}_2$ in the second phase. Thus, if a total ToF is provided as an input, the problem is fully constrained and the control parameters $\{\bar{\psi}_1,\ \bar{\psi}_2\}$ can be solved for. The final expression for ΔV from [20] for this transfer strategy is presented in Eq. 15.

$$\Delta V_{\phi_3} = \sqrt{\frac{\mu}{\bar{a}_0}} - \sqrt{\frac{\mu}{\bar{a}_f}} + \frac{\bar{\psi}_2}{\sin\psi_2}\sqrt{\frac{\mu}{\bar{a}_f}}\left(\bar{i}_f - \bar{i}_0\right) \tag{15}$$

3.2 Guidance Algorithm for Elliptical Orbits, ϕ_4

While the methods in the previous section were effective at estimating ΔV for low-thrust transfer between circular Earth orbits, they are not applicable for transfer to, from, and between elliptical orbits. As a result, the implementation of a computationally efficient guidance law is warranted. When nonconservative perturbations such as thrusting are involved, one common method for describing the effects of perturbations on the evolution of an orbit is through Gauss' variational equations (GVE). These equations express the rate of change of the classical orbital elements $\{a,\ e,\ i,\ \Omega,\ \omega,\ \nu\}$ as a function of the perturbing accelerations $\mathbf{f} = [f_R,\ f_T,\ f_N]^T$, where $\mathbf{f}$ is expressed in the radial-transverse-normal (RTN) reference frame of the satellite. Using the GVEs however, present numerical issues as they become singular for circular and equatorial orbits. To overcome these issues, it has been common to adopt the set of modified equinoctial elements $\{p,\ f,\ g,\ h,\ k,\ L\}$, defined in [23], and describe the dynamics by differentiating those expressions in terms of time [24]. The outcome of this is a dense dynamic model structure comprised of a set of highly coupled differential equations, where the evolution of each modified equinoctial element is a function of the true longitude L [24] and all, but the semiparameter p, are affected by the normal component of the perturbing acceleration. For these these reasons, we are motivated to replace the use of modified equinoctial elements to with a set of nonsingular *ideal elements* proposed by Leomanni et al. [22] to describe orbital motion. This set of elements, inspired by use of *Hansen's ideal frame*, is defined by Eq. 16.

$$\begin{aligned}
\rho &= p/R_e \\
\sigma &= L - s \\
e_x &= f\cos(\sigma) + g\sin(\sigma) \\
e_y &= -f\sin(\sigma) + g\cos(\sigma) \\
h_x &= h\cos(\sigma) + k\sin(\sigma) \\
h_y &= -h\sin(\sigma) + k\cos(\sigma) \\
\sigma &= L - s
\end{aligned} \tag{16}$$

As demonstrated through their study [22], employing this set of elements possesses the following numerical benefits:

- The proposed *ideal anomaly*, s, is observed to be the fictitious time from the Sundman transformation $\mathrm{d}t = \alpha r^n\,\mathrm{d}s$ of the form $n = 2$, and $\alpha = 1/h$ in the unperturbed case. As the dynamics of s are not affected by perturbing accelerations, it is an attractive basis for regularization.
- Regularizing the equations of motion can increase the accuracy and speed of the numerical integration [25].
- The resultant dynamic model structure with ideal elements exhibit a high level of sparsity when compared to other element sets, reducing the computational load required to solve or approximate the optimal control problem.

For these reasons, the dynamic model employed for this work will follow the J_2 perturbed regularized formulation introduced in [22] and adopt the Q-law inspired Lyapunov guidance scheme in Eq. 17 to resolve the transfer maneuvers involving elliptical orbits. In contrast to the Q-law quantifying the "best-case quadratic time-to-go", this candidate Lyapunov function attempts to quantify the ΔV required to bring the spacecraft orbit to the desired target [22], making it an attractive strategy for the global optimization problem. This method makes use of three orbital parameters γ, λ_1, λ_2 introduced in [26] to describe the relative inclination, and relative angles between the chaser spacecraft and target debris orbit periapsis with respect to point in which the two orbit planes intersect, respectively. The Lyapunov candidate function can therefore be defined as:

$$V(\mathbf{y}) = \frac{k_a}{2}\sqrt{\frac{\mu}{\bar{a}}}\left(\sqrt{\frac{\bar{a}}{a}}-1\right)^2 + \sqrt{\frac{\mu}{a(1-e^2)}}\left[k_e\frac{\|\mathbf{e}\|^2}{2} + k_\gamma \tan^2\left(\frac{\gamma}{2}\right)\right] \tag{17}$$

where

$$\mathbf{y} = \begin{bmatrix} a & e & \gamma & \lambda_1 & \lambda_2 \end{bmatrix}^T \tag{18}$$

$$\mathbf{e} = \begin{bmatrix} e\cos(\lambda_2) - \bar{e}\cos(\lambda_1) \\ e\sin(\lambda_2) - \bar{e}\sin(\lambda_1) \end{bmatrix} \tag{19}$$

with $\bar{a}$ and $\bar{e}$ representing the semimajor axis and eccentricity of the target orbit, respectively. This guidance law is used in two stages of the framework. It is selectively called in the first stage for the ΔV and time estimation of transfers involving elliptical orbits, and once again in the last stage to refine the optimization of the trajectories in the converged sequence. When it is used in the first stage of optimization, the weighting parameters $k_a,\ k_e,\ k_\gamma \geq 0$ are static, with values informed by the relative magnitudes of the terms in Eq. 17. When this guidance law is revisited in final stage of the framework, these weighting parameters are dynamically tuned using a gradient-based method.

4. SOLUTION PROCEDURE

4.1 Time-Dependent Cost Generation

The first stage generates a two-dimensional approximation of the time-dependent search space for each departure-arrival debris pair ij. To provide an account for the effect of the departure epoch and transfer duration on the transfer cost, an array of sample departure epochs τ_d with a user-defined time resolution is used to generate a set of ephemerides for each debris object. For each $t_{d,i} \in \tau_d$, the state vector of both departure and arrival targets are fed into the transfer cost module, containing implementations of the transfer strategies $\{\phi_1,\ \phi_2,\ \phi_3,\ \phi_4\}$, for cost estimation. The output of this transfer cost estimation is a 2-dimensional description of the maneuver cost in a space spanned by τ_d and τ_a for each departure/arrival debris pair. Saving this discretized representation of the problem space concludes the first stage of the optimization framework.

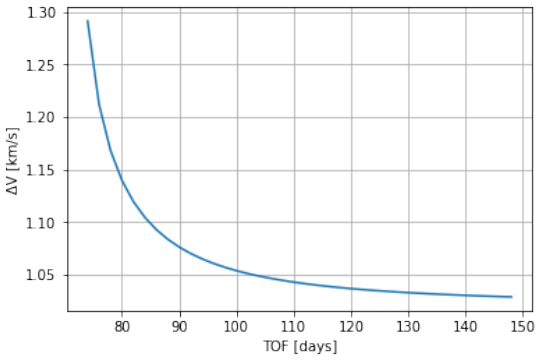

Fig. 1: $\Delta V_{\phi_1} = f(ToF)$

From an intermediary result shown in Figure 1, it is observed that the ΔV costs decrease asymptotically as the time of flight increases. This represents a region of diminishing returns, as the chaser spacecraft will only save a marginal amount of fuel despite adding weeks to the total transfer time. Consistently choosing the absolute minimum ΔV of all

the transfer options and transfer times can be problematic as this can lead to a violation of the overall mission time constraint. One can select the upper bound on the flight time to be sufficiently small to mitigate this, but asserting a uniform constraint for all possible transfer pairs can over-constrain the TPBVP for some transfer pairs, resulting in a loss of optimal solutions. Thus, there is a need to assess the trade-off between flight time and ΔV within the transfer module. A simple method to accomplish this is with a linear weighting function. A weighting function uses coefficients to determine the relative contribution of one parameter with respect to another in the overall objective function. Adjustments to these coefficients reflect a change in relative preference of priority. The cost of a transfer is therefore calculated with the weighting function presented in Equation 20. w can be thought of as a scaling factor for ΔV such that ΔV and time of flight $ToF = t_{a,j} - t_{d,i}$ are of similar magnitudes. The user can initialize w to their preference, and the optimizer will adjust this value if the relative emphasis leads to a violation of overall mission constraints.

$$c_{ijk}(t_{d,i},\, t_{a,j},\, \phi_k) = w\Delta V_{\phi_k}(t_{d,i},\, t_{a,j}) + [t_{a,j} - t_{d,i}] \tag{20}$$

4.2 Global Optimization with the Genetic Algorithm

As the search space grows factorially with the number of debris objects to sequence, the second stage employs a genetic algorithm (GA) to search the discretized problem space and optimally sequence the debris object list. GA draws inspiration from the natural selection process, using biologically inspired operators to improve the fitness of a population over time. The genetic algorithm begins with a randomly generated population containing m trial solutions, where m is an integer defined by the user. The fitness of each trial solution is negatively correlated with the total maneuver cost of that mission sequence, such that sequences that have higher ΔV requirements will have a lower fitness value. Each major iteration of the GA instance is called a generation. In a generation, the population is first passed through a parent selection operator, crossover operator, and lastly the mutation operator. The output at the end of each generation is a new set of individuals to constitute the population in the next generation.

Evaluating the trade-offs between solution space exploration, exploitation, computational complexity, and overall simulation convergence, the rank selection operator was chosen for this implementation of the GA. With this operator, the probability for selecting an trial sequence to construct the next generation is proportional to their rank in fitness, normalized by the size of the population. The benefit of this operator over its alternatives is that a rank-based probability prevents highly fit sequences from saturating the fitness pool, thereby providing a consistent method to distinguish the fitness of trial sequences in a population. The balance between solution exploration and fitness exploitation is also constant with each successive generation. This property is a shortcoming of the rank selection operation, as it is desirable to value exploration more than exploitation early on in the optimization procedure. This effect will be offset through an adaptive mutation operator.

The crossover operator key to the optimization process as it prescribes how new trial solutions are generated from the previously selected sequences. In effort to increase the fitness of the next generation, information regarding the effects of certain segments on the parent's overall fitness and the sensitivity of the segment's cost with respect to time must advise the crossover process. A departure/ arrival debris pair can have a transfer cost of c_{ijk_1} if the transfer maneuver was initiated at $t_{d,i} = epoch_1$ but can have an entirely different cost c_{ijk_2} if the transfer was initiated several weeks later. To capture the magnitude and sensitivity of a given departure/ arrival debris pair's transfer cost as it effects the overall fitness of the sequence, a proprietary crossover algorithm was developed using the statistical properties of the transfer cost to construct new trial sequences.

4.3 Optimization Execution

The fitness for each trial solution, a debris sequence, is assembled through a series of searches in the hash table generated by the optimal trajectory estimation scheme. The first transfer maneuver occurs at the start of the mission window and the state vector describing the chaser spacecraft is equivalent to that of the first debris object. The function finds the departure/arrival debris pair using a corresponding key, then keys in the departure epoch to obtain the optimal cost, ΔV, and time of flight associated with that segment. The time of flight and minimum service time is added to the current mission time to set the departure epoch for the next transfer segment. As the range of departure epochs are sampled discretely, the program will select the next closest sample epoch. The state vector of the chaser spacecraft is subsequently updated to reflect that of the arrival debris at the current mission time. The arrival debris becomes the departure debris and the next object in the sequence is the arrival target. This process continues, accumulating the cost of each segment until the sequence has been enumerated. As the GA maximizes fitness, the fitness value is some ceiling number minus the total cost of the segment. If at any point in this process, constraints on the total mission

time or total ΔV expenditure are violated, the function will adjust the weighting value w of the cost function, and call the trajectory optimization module with the adjusted w to find new optimal solutions. If the GA optimization is determining the fitness of the last generation, the guidance control law is called in the loop to refine the final optimized trajectories and departure epochs. This is the third and final stage of the optimization framework. The spacecraft mass is adjusted after the completion of every segment to reflect the decrease in total mass due to the deployment of a de-orbiting kit and propellant expenditure. This update to the spacecraft mass will increase the thrust acceleration in subsequent transfers, decreasing the ΔV requirement when compared to first-stage estimates. Figure 2 is a flow diagram illustrating the execution process of this optimization framework.

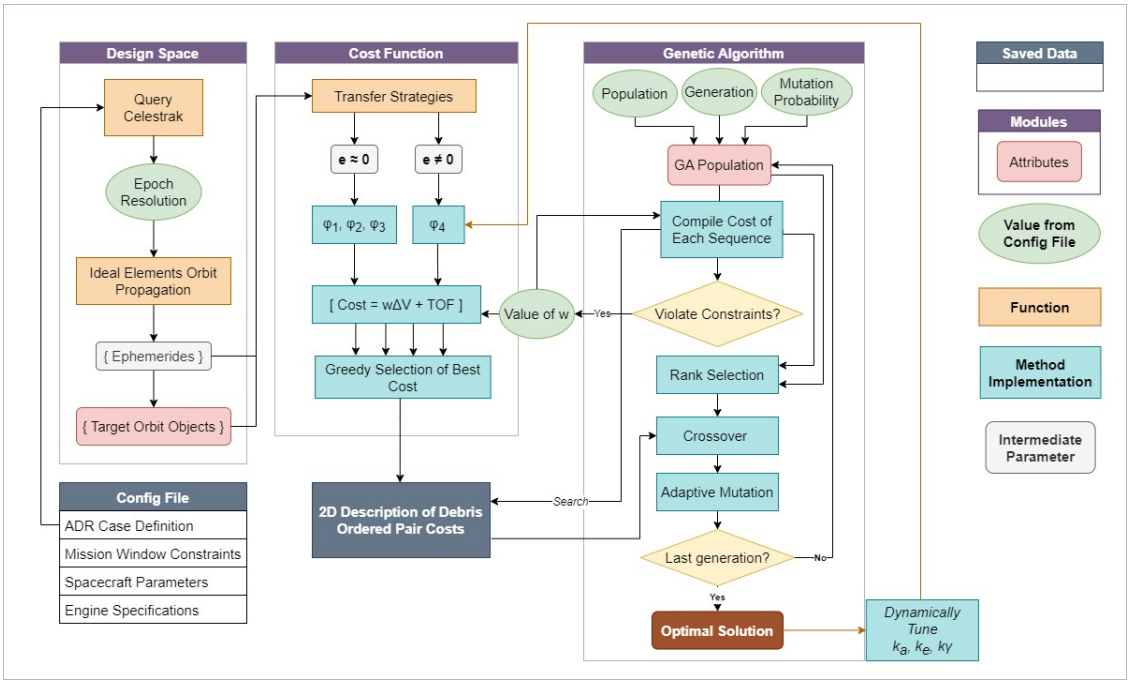

Fig. 2: Diagram of the optimization framework developed for optimal ADR mission planning

5. SIMULATION AND RESULTS

The results of three case studies are presented to demonstrate the validity of the proposed optimization framework. The first two case studies replicate the mission scenarios investigated by two other researchers. The results obtained from running cases on these mission scenarios are compared against the published research results. The last case study considers the optimization of an arbitrary set of debris targets with a reasonable Δi range and e variability amongst the target orbits. The purpose of this case study is to demonstrate the optimization framework's ability to sequence debris target lists with a variety of orbit inclinations, a capability that is not prevalent in the solution methods found in literature. The optimization of these cases were performed on a machine with an Intel Core i7 CPU processor and 16 GB RAM under the 64-bit Windows 11 operating system.

5.1 Case 1: Comparing Optimal Results with a Low-Thrust MTRV ADR Study

The first case study compares the results obtained from the developed optimization framework with that from another study considering the optimal planning of a **low-thrust** ADR mission in LEO [4]. The carrier spacecraft in this reference study is 2750 kg and equipped with a 100 mN thruster capable of 1600s of I_{sp}. Each deorbiting kit has a mass of $m_{deorbiter}$=175 kg. Table 1 tabulates the list of debris objects to sequence, along with the relevant classical orbital elements at the beginning of the mission window. It is noted that the selected debris objects are in very similar orbits. The GA was initialized with a population size of 200, iterated over 50 generations, with adaptive mutation probabilities between 30% and 75%. 10 independent GA instances were executed to confirm the reliability of the optimized sequence.

Table 1: List of debris objects for Case 1 [4]

NORAD	a [km]	e	i [deg]	Ω [deg]
39011	7468.35	0.0083	63.3835	237.2911
39012	7468.35	0.0083	63.3824	237.3044
39013	7468.34	0.0083	63.3851	236.4881
39015	7472.54	0.0095	63.3828	246.1591
39016	7471.19	0.0097	63.3825	240.6863
40338	7468.31	0.0010	63.4108	239.8075
40339	7468.31	0.0010	63.4097	239.8082
40340	7468.32	0.0010	63.4084	240.6788
40342	7473.24	0.0019	63.4096	240.8979
40343	7471.88	0.0020	63.4093	245.3040

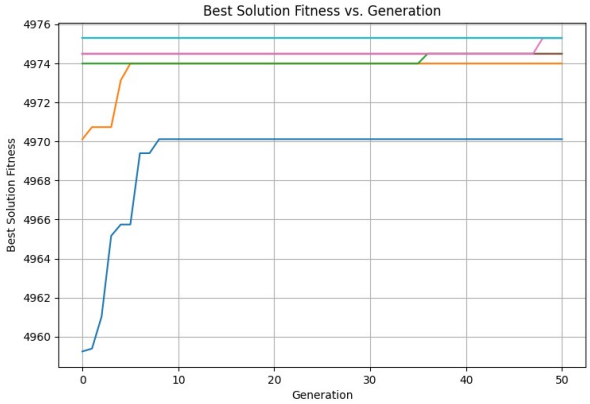

Fig. 3: 10 independent GA instances for Case 1

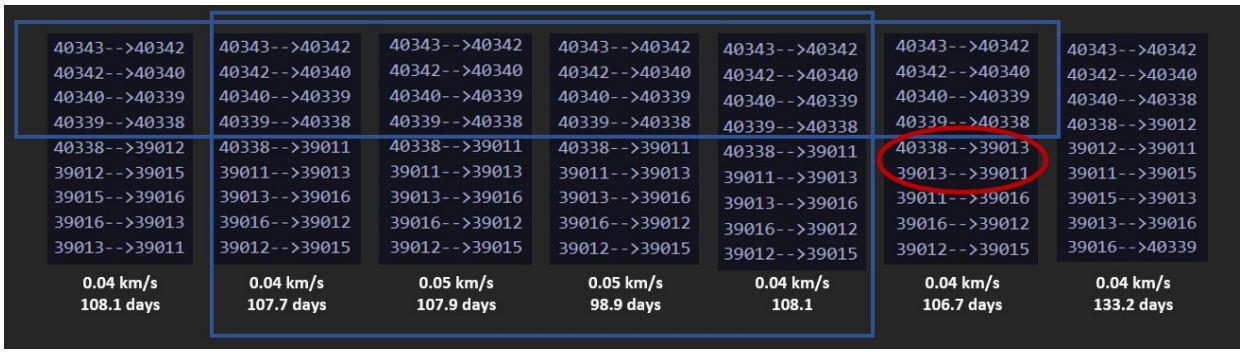

Fig. 4: Optimized sequences from 7 of 10 independent GA runs

The progression of the best solution's fitness during each of the 10 independent GA instances is summarized by Figure 3. It is observed that majority of the improvements in fitness occur within the first 10 generations before saturating at a maximum. With several independent runs, the program can evolve different initial populations to try and reach the same objective. Figure 4 details the final sequence obtained by the GA for 7/10 independent runs. It is observed that for 10/10 of the runs, the first two transfer segments are identical. Indicated by the blue boxes, 6/10 runs sequenced the first 4 transfer segments consistently, while 4/10 runs produced the same final sequence with minor variation on the total ΔV and mission duration. The champion result (second to the right) is very similar to those of these 4 GA instances, with the exception of the two circled segments. Swapping 39011 with 39013 saves one day for the mission, which is not a significant difference since the total mission duration allocated is 365 days. These results demonstrate that the framework is effective at consistently converging to the global optimum.

The champion result is detailed on the left half of Table 2 below. The corresponding ΔV and time of flight for each transfer segment of the mission are also presented. The right half of this table summarizes the solution results from the reference study. It can be observed that with the adopted transfer strategy, the solution framework outputs a sequence that requires 88% less ΔV and completes the mission in almost 1/3rd of the time when compared with the published result. The difference in final spacecraft mass, m_f, between these two results indicates that 208.1 kg of propellant is saved with the devised optimization strategy. In addition to using a minimum ΔV scheme, another explanation for the discrepancy between these two results is that the reference study assumed that the transfer costs were independent of time. Although the orbits of the debris objects are very similar, the solution framework may have detected certain transfer segments for which the $\Delta\Omega$ is reduced after some passage of mission time due to the J_2 perturbation.

Table 2: Comparison between the proposed framework result and the published result for Case 1

	Solution framework results				**Published results** [4]			
	Departure	Arrival	ΔV [km/s]	ToF [days]	Departure	Arrival	ΔV [km/s]	ToF [days]
1	40343	40342	0.0023	2.58	39013	39011	0.010	51
2	40342	40340	0.0103	4.5	39011	39012	0.004	10
3	40340	40339	0.0021	4.5	39012	39016	0.093	27
4	40339	40338	0.0045	4.5	39016	40342	0.044	31
5	40338	39013	0.0050	9.1	40342	40340	0.013	32
6	39013	39011	0.0009	4.5	40340	40339	0.024	43
7	39011	39016	0.0051	4.5	40339	40338	0.003	2
8	39016	39012	0.0090	5.0	40338	40343	0.114	52
9	39012	39015	0.0021	4.5	40343	39015	0.042	54
Total			**0.0413**	**106.7**			**0.3470**	**302**
	m_0 = 2750 kg		m_f = **1170 kg**		m_0 = 2750 kg		m_f = **961.9 kg**	

5.2 Case 2: Comparing Optimal Results with a High-Thrust MTRV ADR Study

The second case study compares the results obtained using the devised solution framework with that from a study considering the optimal planning of a **high-thrust** ADR mission in LEO [3]. The carrier spacecraft in this reference study is 7000 kg and each deorbiting kit has a mass of 30 kg. To evaluate the performance of this ADR mission with a low-thrust propulsion system, the thruster is assumed to produce 449 mN of thrust and 2219s of I_{sp}. Table 3 tabulates the list of debris objects to sequence, along with the relevant classical orbital elements at the beginning of the mission window. These objects were randomly selected from the Iridium 33 debris cluster by the researchers of this study, and thus like Case 1, share very similar orbital elements.

The GA parameters are identical to those used to optimize Case 1, demonstrating the robustness of this algorithm. The sequence that yields the highest fitness is detailed on the left half of Table 4 below. The corresponding ΔV and time of flight for each transfer segment of the mission are also presented. The right half of this table summarizes the solution results from the reference study. The highlighted results indicate that the use of low-thrust propulsion for this ADR mission can reduce the propellant consumption by 43.8% while only adding 1.5 months to the total mission time frame. In terms of absolute values, switching to low-thrust propulsion can allow for 2048 kg of mass savings in propellant alone. If one were to use the current (2022) Falcon 9 launch prices of $2938 per kg [27], the significance of this mass saving is a $6 million reduction in launch costs.

Table 3: List of debris objects for Case 2 [3]

NORAD ID	a [km]	e	i [deg]	Ω [deg]
33886	7153.0	0.0012	86.3810	265.1455
33773	7133.0	0.0011	86.3999	261.0980
34160	7088.0	0.0055	86.4029	241.5819
33870	7148.0	0.0022	86.3770	262.0968
34367	7125.0	0.0026	86.4112	241.1697
33878	7181.0	0.0104	86.3073	239.4547
34378	7122.0	0.0055	86.3530	237.7939
33953	7143.0	0.0024	86.3905	261.3071
35297	7161.0	0.0016	86.3867	266.6037

Table 4: Comparison between the proposed framework result and the published result for Case 2

	Solution framework results				**Published results** [3]			
	Departure	Arrival	ΔV [km/s]	ToF [days]	Departure	Arrival	ΔV [km/s]	ToF [days]
1	33878	33870	0.0302	9.56	33773	34378	0.2912	0.6
2	33870	33953	0.0147	5.0	34378	33886	0.0581	0.56
3	33953	33886	0.0126	3.0	33886	33878	0.0603	1.29
4	33886	35297	0.0031	1.63	33878	34367	0.1528	1.33
5	35297	34367	0.0234	14.56	34367	33953	0.0348	0.4
6	34367	34160	0.0055	9.56	33953	33870	0.0554	0.76
7	34160	34378	0.0228	4.56	33870	34160	0.1973	1.22
8	34378	33773	0.0060	4.56	34160	35297	0.0366	0.32
Total			**0.1192**	**52.4**			**0.8865**	**6.48**
	m_0 = 7000 kg		m_f = **6723 kg**		m_0 = 7000 kg		m_f = **4675 kg**	

5.3 Case 3: Optimizing a Set of Debris in LEO, MEO, and GTO

Lastly, as the other two case studies only considered the sequencing of debris objects in very similar orbits, this case considers optimizing the removal sequence of a set of debris objects in LEO, MEO, and GTO to showcase the true flexibility of the developed optimization framework. Table 5 tabulates the list of debris objects to sequence, along with the relevant classical orbital elements at the beginning of the mission window. The mission scenario is modeled according to the Deorbiter Cubesat mission [19]. The mothership for this ADR mission is a mid-sized 1000 kg spacecraft equipped with a BHT-8000 hall-effect thruster that can produce 449 mN of thrust with an average I_{sp} of 2219s. The Deorbiter CubeSats onboard the mothership have a total wet mass of 16 kg. The maximum mission duration is 2 years, and the minimum time allocated to characterize the dynamical state of the target debris is 7 days. Table 5 tabulates the list of debris objects to sequence, along with the relevant classical orbital elements at the beginning of the mission window. The GA was initialized with a population size of 100, iterated over 100 generations, with adaptive mutation probabilities between 30% and 75%. Again, 10 independent GA instances were executed to confirm the consistency of the optimized sequence.

Table 5: List of debris objects for Case 3

NORAD ID	a [km]	e	i [deg]	Ω [deg]	ω [deg]	Orbit Type
20323	7096.8611	0.0075	97.1936	69.4811	265.7741	LEO
22970	7563.8736	0.0020	82.6128	156.0112	358.5592	LEO
27463	24477.577	0.7177	4.5672	286.7717	89.0267	GTO
43248	28790.512	0.0095	55.6052	0.8142	14.2856	MEO
39081	17877.497	0.6272	6.4476	168.5245	12.6117	MEO
28379	25930.027	0.7321	7.3560	113.9091	110.3966	GTO

The progression of best solution fitness over the generations for each of the 10 independent GA instances is summarized by the plot presented in Figure 10. It was observed that the final fitness value of the best solution is consistent across all 10 independent GA instances. The case is seen to converge very rapidly, with all of the improvements occurring within the first 2 generations before stagnating at the final fitness value of 4113. This indicates that the search space for this debris set either contains few local optimums or contains local optimums that all possess the same fitness value. As can be observed in Figures 5 through 9, the genetic algorithm identified that the most efficient way to visit the 2 distinct GTOs is done not by visiting them consecutively. Rather, it is to start at the orbit of 27463, leverage the orbit evolution of the elliptical MEO of 39081 caused by the J2 perturbation to finally achieve a closer alignment with

the other GTO (28379). The chaser spacecraft then begins visiting successively lower altitude orbits, reaching another MEO target, and finally, deorbiting the 2 debris targets in the low-earth orbits. The result of this novel ADR case study is that 6 debris objects with an altitude range of 7097 km to 28,790 km, inclination spread of 4 degrees to 97 degrees, and eccentricity values of 0.00 to 0.73 can be removed in 593 days with 13.6 km/s of ΔV.

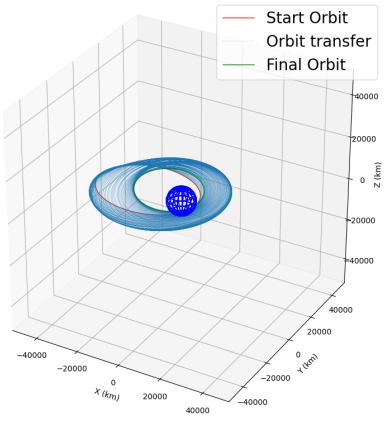

Fig. 5: (GTO) 27463→ 39081 (MEO) at $t_{d,1} = 2022\text{-}01\text{-}01$

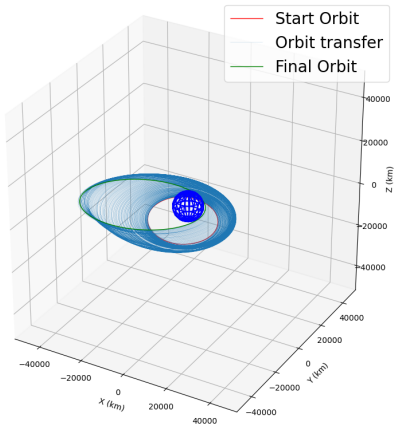

Fig. 6: (MEO) 39081→ 28379 (GTO) at $t_{d,1} = 2022\text{-}04\text{-}20$

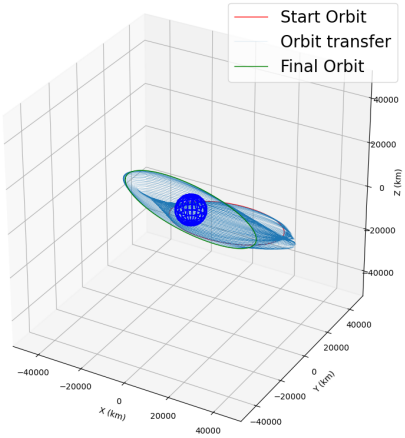

Fig. 7: (GTO) 28379→ 43248 (MEO) at $t_{d,1} = 2022\text{-}08\text{-}15$

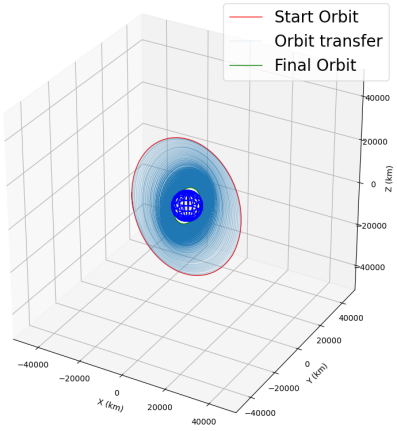

Fig. 8: (MEO) 43248→ 22970 (LEO) at $t_{d,1} = 2022\text{-}11\text{-}22$

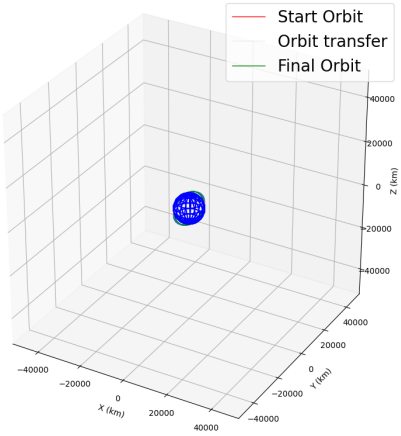

Fig. 9: (LEO) 22970→ 20323 (LEO) at $t_{d,1} = 2023\text{-}04\text{-}08$

To contextualize the significance of this result, the first transfer segment, 27463→ 39081, alone can require up to 11.3 km/s of ΔV if it were initiated 560 days into the mission. The second transfer segment, 39081→ 28379, would require 4x the amount of ΔV and over 2x the transfer time – 4.25 km/s and 187 days, respectively– if it were the first transfer planned in the debris removal sequence. Table 6 displays the ΔV and time of flight for each transfer segment of the optimized sequence when contrasted against the highest possible transfer cost in the mission window. It shall be noted that these worst-case transfer costs are only associated with the segments of the converged optimal sequence. Other possible departure/arrival debris pairs likely possess even greater transfer costs and variability with time.

The results from this case study demonstrate the novel accomplishment of the proposed optimization framework – that it can effectively optimize an arbitrary set of debris objects ***without any restrictions placed on the properties of the target debris' orbits***, enabling substantial reduction in terms of propellant requirements and mission duration.

Table 6: Solution framework results for a variety of orbits not limited to LEO

	Solution framework results				**Worst-case transfer**		
	Departure	Arrival	ΔV [km/s]	ToF [days]	ΔV [km/s]	ToF [days]	Days into Mission
1	27463	39081	2.2872	96.3	11.277	406.6	560
2	39081	28379	1.6078	85.8	4.2480	187.5	0
3	28379	43248	3.0193	111.2	3.6423	133.7	100
4	43248	22970	4.4615	187.2	4.4660	187.7	332
5	22970	20323	2.2395	77.6	2.2734	79.0	116
Total			**13.62**	**593.2**	**25.91**	**994.5**	
	m_0 = 1000 kg		m_f = **510 kg**				

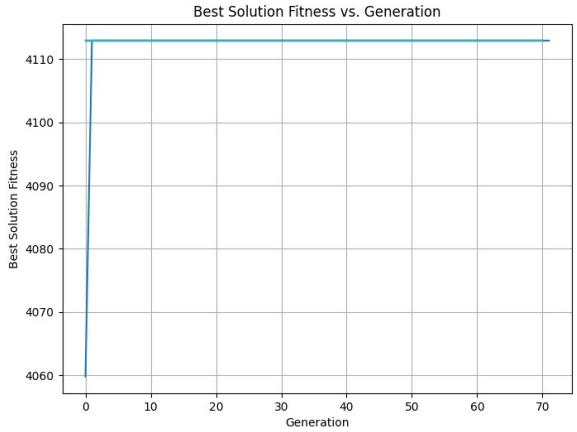

Fig. 10: Best solution fitness vs. Generation of 10 independent GA runs for Case 3

6. CONCLUSION

In this research, a framework to optimize the MTRV problem for low-thrust ADR missions that remove several specific debris objects of interest was developed. This framework relaxed the coupling of the nonlinear trajectory optimization from the combinatorial optimization by decomposing the problem into three stages. The first stage was aimed at estimating the transfer cost of the optimal long-range rendezvous trajectory between a given departure/arrival debris pair, as a function of time. The estimation of the optimum was performed by considering 4 distinct transfer strategies, and their variations as a function of departure and arrival epoch. Another account for time dependency was the consideration on how these costs vary with different departure epoch, and identifying which transfer pairs were more sensitive to this effect than others. The ΔV for a given transfer maneuver was seen to asymptotically approach a minimum for longer permitted transfer times, demonstrating a case of diminishing returns. A weighted cost function was thus introduced to evaluate the trade-off between these competing objectives. The output of the first stage was a hash table containing ΔV and flight time for the lowest cost transfer for all departure/arrival debris pairs at all departure epochs. The second stage of the framework employs a Genetic Algorithm to optimize the debris sequence. Information regarding the sensitivity of the departure/arrival debris pairs on departure epoch are embedded in the crossover scheme, and the fitness value is calculated by accumulating the cost of each transfer segment and subtracting the total from some bounding value. The mission window constraints and total ΔV constraints trigger the program to automatically adjust the weighting parameter and re-evaluate transfer optimums. The last stage takes the final sequence from the genetic algorithm and refines the transfer trajectories and maneuver epochs by resolving each transfer segment with a Lyapunov-based guidance law. The gains in the Lyapunov candidate function are tuned dynamically with a gradient-based method to refine the transfer trajectories and maneuver epochs in order to better resolve the optimal solution.

It was demonstrated that this framework required relatively low computational resources as the optimization of a 10 debris object case with a 1 year mission window and 4 day epoch resolution could be completed within 45 minutes. The outcome of this work is a modular, adaptive framework that can optimize the debris removal sequence of a variety of ADR mission scenarios utilizing low-thrust propulsion.

7. REFERENCES

[1] J. C. Liou and N. L. Johnson, "A Sensitivity Study of the Effectiveness of Active Debris Removal in LEO," *Acta Astronautica*, vol. 64, no. 2, pp. 236–243, 2009.

[2] J. C. Liou and N. L. Johnson, "Risks in Space from Orbiting Debris," *Science*, vol. 311, pp. 340–341, 2006.

[3] J. Bang and J. Ahn, "Multitarget Rendezvous for Active Debris Removal Using Multiple Spacecraft," *Journal of Spacecraft and Rockets*, vol. 56, no. 4, pp. 1237–1247, 2019.

[4] J. M. R. M. Marilena Di Carlo and M. Vasile, "Automatic Trajectory Planning for Low-Thrust Active Removal Mission in Low-Earth Orbit," *Advances in Space Research*, vol. 59, no. 5, pp. 1234–1258, 2017.

[5] N. Bérend and X. Olive, "Bi-objective Optimization of a Multiple-target Active Debris Removal Mission," *Acta Astronautica*, vol. 122, pp. 324–335, 2016.

[6] Y. Y. H. L. Tianjiao Zhang, Hongxin Shen and J. Li, "Ant Colony Optimization-based Design of Multiple-target Active Debris Removal Mission," *Advances in Space Research*, vol. 61, no. 5, pp. 201–210, 2018.

[7] H. L. Shiyu Chen, Fanghua Jiang and H. Baoyin, "Optimization for Multitarget, Multispacecraft Impulsive Rendezvous Considering J2 Perturbation," *Journal of Guidance, Control, and Dynamics*, vol. 44, no. 10, pp. 1811–1822, 2021.

[8] I. J. Christoph Hansknecht and S. Stiller, "Dynamic Shortest Paths Methods for the Time-Dependent TSP," *Algorithms*, vol. 14, no. 21, pp. 1–23, 2021.

[9] F. Zuiani and M. Vasile, "Preliminary Design of Debris Removal Missions by Means of Simplified Models for Low-Thrust, Many-Revolution Transfers," *International Journal of Aerospace Engineering*, no. 836250, 2012.

[10] S. C. Haiyang Li and H. Baoyin, "J2-Perturbed Multitarget Rendezvous Optimization with Low Thrust," *Journal of Guidance, Control, and Dynamics*, vol. 41, no. 3, pp. 2151–2171, 2018.

[11] M. Cerf, "Multiple Space Debris Collecting Mission: Optimal Mission Planning," *Journal of Optimization Theory and Applications*, vol. 167, no. 1, pp. 195—218, 2015.

[12] T. N. Edelbaum, "Propulsion Requirements for Controllable Satellites," *American Rocket Society Journal*, vol. 31, no. 8, p. 1079–1089, 1961.

[13] S. F. J. G. M. M. C. K. C. W. Vitali Braun, A. Lüpken and P. Vörsmann, "Active Debris Removal of Multiple Priority Targets," *Advances in Space Research*, vol. 51, no. 9, pp. 1638–1648, 2013.

[14] X.-q. C. Jing Yu and L. hu Chen, "Optimal Planning of LEO Active Debris Removal Based on Hybrid Optimal Control Theory," *Advances in Space Research*, vol. 55, no. 11, pp. 2628–2640, 2015.

[15] Y. L. Jianan Yang, Yu Hen Hu and Q. Pan, "A Maximal-Reward Preliminary Planning for Multi-Debris Active Removal Mission in LEO with a Greedy Heuristic Method," *Acta Astronautica*, vol. 149, pp. 123–142, 2018.

[16] X. H. Yang Zhou, Ye Yan and L. Kong, "Mission Planning Optimization for Multiple Geosynchronous Satellites Refueling," *Advances in Space Research*, vol. 56, no. 11, pp. 2612–2625, 2015.

[17] L. C. Hong-Xin Shen, Tian-Jiao Zhang and D. Pastrone, "Optimization of Active Debris Removal Missions with Multiple Targets," *Journal of Spacecraft and Rockets*, vol. 55, no. 1, pp. 181–189, 2018.

[18] A. M.-D. K. Daneshjou and M. Bakhtiari, "Mission Planning for On-Orbit Servicing Through Multiple Servicing Satellites: A New Approach," *Advances in Space Research*, vol. 60, no. 6, pp. 1148–1162, 2017.

[19] H. Hakima and M. R. Emami, "Deorbiter CubeSat mission design," *Advances in Space Research*, vol. 67, no. 7, pp. 2151–2171, 2021.

[20] M. D. Carlo and M. Vasile, "Analytical solutions for low-thrust orbit transfers," *Celestial Mechanics and Dynamical Astronomy*, vol. 133, no. 33, pp. 1–38, 2021.

[21] R. D. Falck, W. K. Sjauw, and D. A. Smith, "Comparison of Low-Thrust Control Laws for Applications in Planetocentric space," in *50th AIAA/ASME/SAE/ASEE Joint Propulsion Conference*, 2014, p. 3714.

[22] M. Leomanni, G. Bianchini, A. Garulli, R. Quartullo, and F. Scortecci, "Optimal Low-Thrust Orbit Transfers Made Easy: A Direct Approach," *Journal of Spacecraft and Rockets*, vol. 58, no. 6, pp. 1904–1914, 2021.

[23] M. Walker, B. Ireland, and J. Owens, "A Set Modified Equinoctial Orbit Elements," *Celestial mechanics*, vol. 36, no. 4, pp. 409–419, 1985.

[24] R. H. Battin, *An Introduction to the Mathematics and Methods of Astrodynamics*. AIAA, 1999.

[25] J. R. Vicens, "Regularization in Astrodynamics: Applications to Relative Motion, Low-Thrust Missions, and Orbit Propagation," Ph.D. dissertation, Universidad Politécnica de Madrid, 2016.
[26] M. Leomanni, A. Garulli, A. Giannitrapani, and R. Quartullo, "Satellite relative motion modeling and estimation via nodal elements," *Journal of Guidance, Control, and Dynamics*, vol. 43, no. 10, pp. 1904–1914, 2020.
[27] SpaceX. (2022) Capabilties and Services. [Online]. Available: https://www.spacex.com/media/CapabilitiesServices.pdf